Performance and lifetime assessment of reactor wall and nearby components during plasma instabilities

A. Hassanein [a,*], I. Konkashbaev [b]

[a] *Argonne National Laboratory, Argonne, IL 60439, USA*
[b] *Troitsk Institute for Innovation and Fusion Research, Troitsk, Russian Federation*

Abstract

Surface and structural damage to plasma-facing components (PFCs) due to the frequent loss of plasma confinement is a serious problem for the tokamak reactor concept. The plasma energy deposited on these components during loss of confinement causes significant surface erosion, possible structural failure, and frequent plasma contamination. Surface damage consists of vaporization, spallation, and liquid splatter of metallic materials. Comprehensive multidimensional models that include thermodynamics and thermal hydraulics of plasma-facing materials (PFMs), eroded-debris/vapor atomic physics and magnetohydrodynamics (MDHs), resulting photon radiation and photon transport, as well as liquid splashing and brittle destruction of materials, are used self-consistently to evaluate and assess our current understanding of the lifetime of PFMs and the various forms of damage they experience. Models are developed to study the stability of the vapor shielding layer, erosion of the melt-layer, brittle destruction/explosive erosion, and the issues involved therein.   © 1998 Elsevier Science B.V. All rights reserved.

1. Introduction

Damage to plasma-facing components (PFCs) and structural materials due to loss of plasma confinement in magnetic fusion reactors remains one of the most serious concerns for safe, successful, and reliable tokamak operation. Major plasma instabilities consist of hard disruptions, which include thermal and current quench, edge-localized modes, and vertical displacement events (VDEs). The intense plasma energy (10–200 MJ/m^2) that is deposited during these events over short periods (0.1–300 ms) produce severe surface and bulk damage [1].

Surface damage includes high erosion losses due to surface vaporization, spallation, and melt-layer loss. Bulk damage effects include large temperature increases in the structural materials and at the interface between surface coatings and structural materials. These large temperature increases cause high thermal stresses, possible structure melting, and material fatigue and failure.

Other bulk effects of some plasma instabilities, particularly those of longer duration such as VDEs, or those that deposit energy more deeply (e.g., runaway electrons) can cause high heat flux levels in coolant tubes; this may cause burnout of the tubes and lead to significant down times of repair and maintenance [2].

In addition to these effects, the transport and redeposition of the eroded surface materials by vaporization, melt-layer splashing, and macroscopic particle emission to various locations on plasma-facing and nearby components are a major concern for safety, frequent plasma contamination, and successful and prolonged plasma operations after plasma instability events.

It is well known that the initial stage of the energy deposited during hard plasma disruptions will cause sudden formation of a vapor cloud above the exposed area. This vapor cloud, if well confined, will significantly reduce the net energy flux to the original disruption location, thus substantially reducing vaporization losses by orders of magnitude [3]. Detailed physics of plasma/solid–liquid/vapor interactions in a strong and oblique magnetic field have been developed and evaluated in a comprehensive self-consistent manner. Such detailed treatment of magnetohydrodynamics (MHDs) and

---

* Corresponding author. Tel.: +1 630 252 5289; fax: +1 630 252 5287; e-mail: hassanein@anl.gov.

photon radiation transport in the region of the vapor cloud, for example, is very important when determining the net depth of erosion due to surface vaporization [4]. Analysis of the MHD stability of this vapor cloud is likewise quite important in evaluating the lifetime of PFCs during these abnormal events. Models and analysis to study how the vapor loss away from the area of disruption affects PFCs are presented.

The thickness of the melt layer that is developed on metallic PFCs during plasma instabilities is, however, much larger than surface vaporization losses. Under most reactor disruption conditions, thickness of the melt-layer on metallic PFCs can be one to two orders of magnitude greater than surface vaporization losses [3]. Therefore, the dynamic response of liquid metal layers exposed to various forces during the course of disruption is another serious concern. Models to study detailed melt-layer behavior of metallic PFCs during plasma instabilities have been developed and implemented in the SPLASH and the A*THERMAL-S codes [2–6].

Nonmelting materials, such as graphite and carbon-based materials (CBMs), have also shown large erosion losses that significantly exceed losses from surface vaporization. This phenomenon has been observed in several facilities that simulate disruptions by using various techniques, e.g., electron beams [7], lasers [8], and plasma gun and other devices [9–11]. Models to evaluate the effect of brittle destruction during plasma instabilities on the erosion behavior and lifetime of plasma-facing CBMs and nearby components were also developed and implemented in the SPLASH code. Estimated explosive erosion rates of CBMS and lifetime predictions in reactor conditions are also presented.

2. MHD instabilities in vapor clouds

In many applications, the vapor cloud that develops above an exposed target surface during an intense energy deposition is well known to shield the original surface and absorb most of the incident source energy. The vapor cloud plasma in a reactor environment, however, just like the main reactor plasma, is also subject to MHD instabilities and possible loss of vapor confinement away from the incoming main plasma particles during a disruption. Initially, the cold vapor plasma, with low conductivity near the target surface, diffuses freely across magnetic field lines in the normal direction. This expanding vapor plasma is initially heated by the disrupting main-plasma particles and then by electron heat conduction and photon radiation generated at the outermost vapor regions.

As the cloud vapor becomes ionized, it will turn to follow the initial direction B_0 of the magnetic field lines, as shown schematically in Fig. 1. The magnetic field lines are assumed to be frozen into the surface of the

liquid metal layer because of its high conductivity. Near the upper vapor boundary, the magnetic field lines become almost parallel to the vapor surface. As more vapor is emitted from the surface, the expanding dense and cold vapor will sweep and distort the oblique magnetic field lines. Fig. 2 shows the magnetic field diffusion and distortion in a beryllium vapor in relationship to distance normal to the target surface at two disruption times [12]. The expanding vapor plasma distorts the magnetic field lines as it moves in the normal direction.

Because the vapor plasma near the target surface is more dense, i.e., pressure near the target surface is higher during a shorter disruption time, magnetic field strength is sharply decreased to as little as 50% of its initial value. Because of such distortion in magnetic field lines and the resulting curvature that is produced, a flute-type MHD instability can develop in the vapor plasma. Magnetohyrodynamic instability of this type causes the vapor to move away from the exposed surface; therefore, vapor-shielding efficiency is reduced. Behavior of such vapor plasma was observed recently in an inclined magnetic filed during experiments at the MK-200CUSP facility at TRINITI [13]. The inclined magnetic field lines were achieved by tilting the sample relative to the normally incident field lines of this facility. These experiments demonstrated the drift of vaporized material along the sample surface that led to a significant increase in surface erosion.

A preliminary model was developed to study the effects of vapor MHD instabilities during disruptions [12]. Because one side of the magnetic field is attached (target surface) and the other side is free (outer boundary), a balloon mode of the flute instability can arise. The growth rate of the balloon mode instability can be estimated from the equation

$$\gamma = \sqrt{\frac{B^2}{4\pi\rho}\frac{K_\parallel}{R_M}}, \tag{1}$$

where $K_\parallel$ is the instability wave number, ρ the vapor density, and R_M the radius of curvature of the magnetic field lines (see Fig. 1). The wave number is given by $K_\parallel = 2\pi/\lambda_\parallel$, where $\lambda_\parallel$ is the wavelength of the instability. Under typical reactor disruption conditions, the frequency of this instability is calculated to be $\gamma > 10^5$ s^{-1}. Therefore, the necessary characteristic growth time for this instability to arise is $\tau_M = \gamma^{-1} < 10$ µs. This means that the vapor cloud will lose confinement much sooner than the total disruption time $\tau_d > 100$ µs. A turbulence mass diffusion coefficient D_T for vapor loss can be estimated by solving the equation

$$D_T = \lambda_\parallel^2 \gamma. \tag{2}$$

The wavelength of the developed instabilities depends on vapor cloud parameters and the dimensions of the
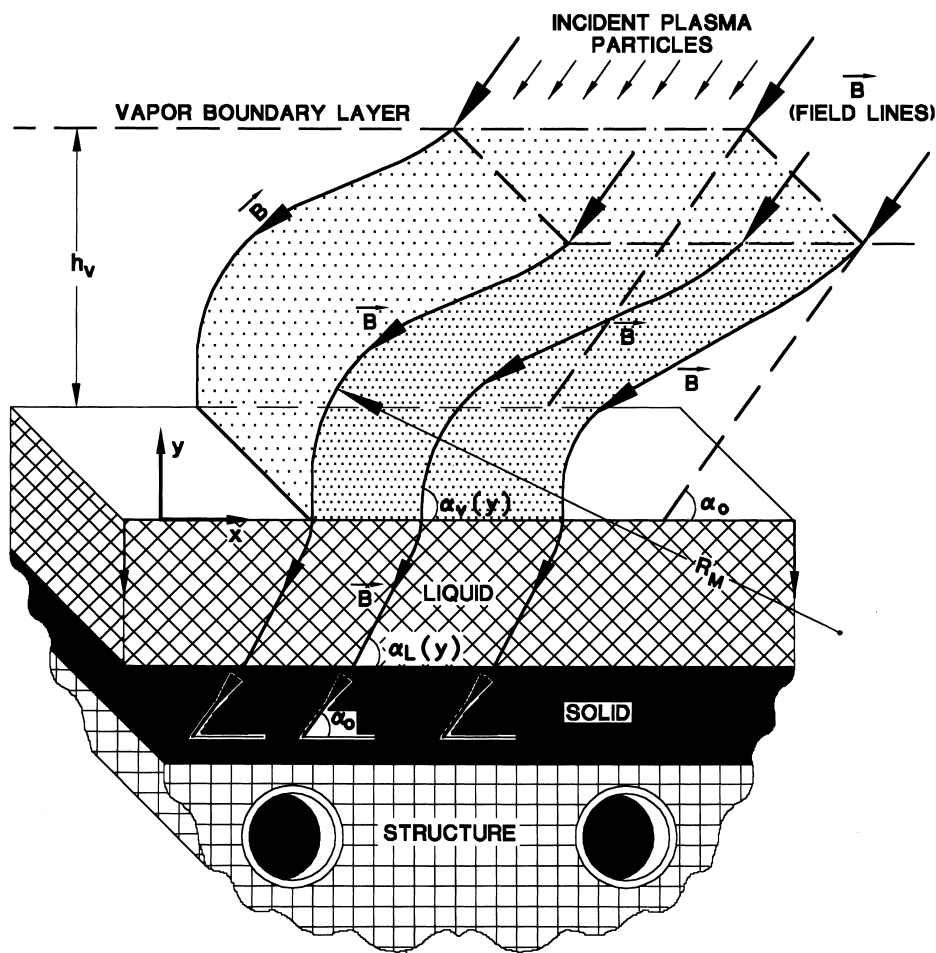
Fig. 1. Schematic illustration of magnetic field diffusion in vapor cloud.

vapor zone above the surface. The model for vapor loss is implemented in the full version of the A*THERMAL-S-2D code, in which the vapor is allowed to be removed laterally along the surface, as well as normal to the exposed surface area. During each time step after the MHD instability has developed, the computer code calculates, for each vapor zone, a net vapor-mass loss that is due to both turbulent MHD diffusion and the classical diffusion across magnetic field lines.

Fig. 3 shows the effect of MHD instabilities on beryllium vapor expansion and vapor temperature as a function of distance normal to the surface at the two indicated disruption times. At the shorter disruption time, the deposited power is greater and causes both the solid/liquid and vapor temperatures to be much higher than those at the longer disruption time. The longer disruption time causes the vapor to expand to greater distances above the target surface and also causes the energy flux deposited at the surface to diffuse deeper into the bulk and produce a thicker melt layer [1].

The oblique magnetic field effectively limits normal vapor expansion to distances <30 cm above the target surface [3]. This is very important in reducing the disruption damage to nearby components from the intense emitted radiation and from vapor deposition [2]. The developed MHD instabilities will, however, limit vapor accumulation above the target surface to ≤ 2 cm before the turbulent vapor will be swept away and disappear from the incoming disrupting plasma particles. However, very little vapor is needed to completely stop the incoming plasma particles and continue shielding the target surface. The turbulent vapor will also take time to leave the disturbed region.

The net erosion rate from surface vaporization that occurs as a result of the MHD instabilities is increased by only a factor of ≤ 2, as shown in Fig. 4, because the turbulent vapor will take time to completely leave the unstable region above the surface. Therefore, despite the MHD instabilities in the vapor plasma and the removal of vapor away from the incident disrupting main plas-
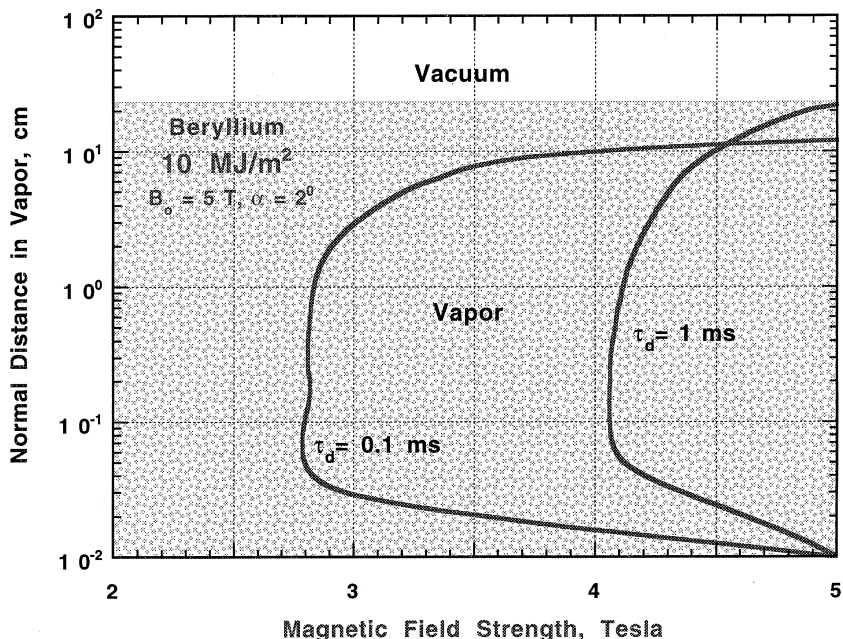
Fig. 2. Magnetic field diffusion in beryllium vapor above target surface for disruption times of 0.1 and 1 ms.
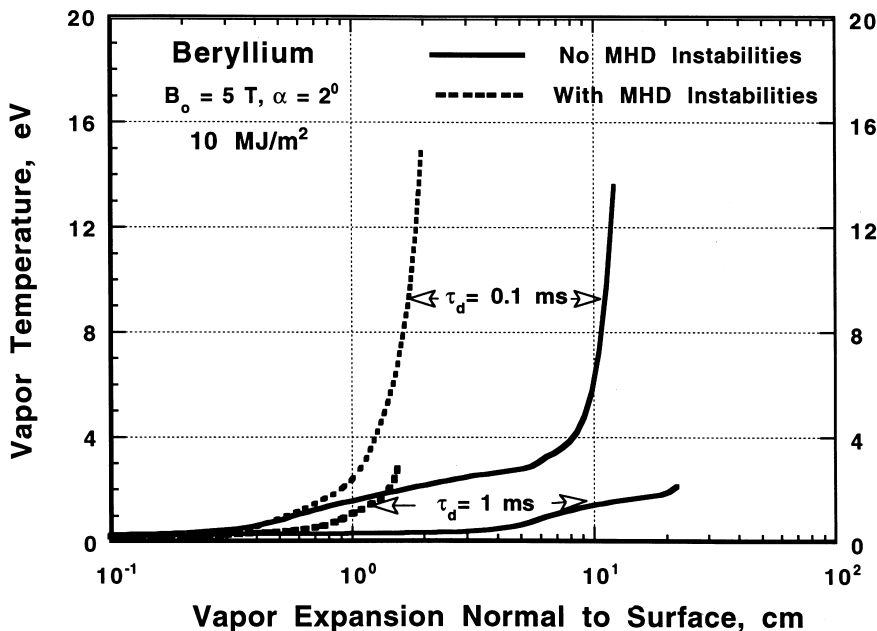

Fig. 3. Effect of MHD instabilities on beryllium vapor expansion normal to surface at two disruption times.

ma, the vapor still offers significant shielding during very short disruption times. For longer disruption times and higher energy deposition, the erosion rate due to vapor loss may, however, increase significantly.

Because of the loss of vapor confinement, the diffusing hot turbulent vapor will deposit its energy on nearby components and thus cause more erosion. The overall net erosion rate will depend on the parameters of the disrupting plasma, the size of the disruption spot, design configuration, and the type of PFM. However, for more accurate assessment of such damage, a full two-dimensional analysis with realistic plasma-facing
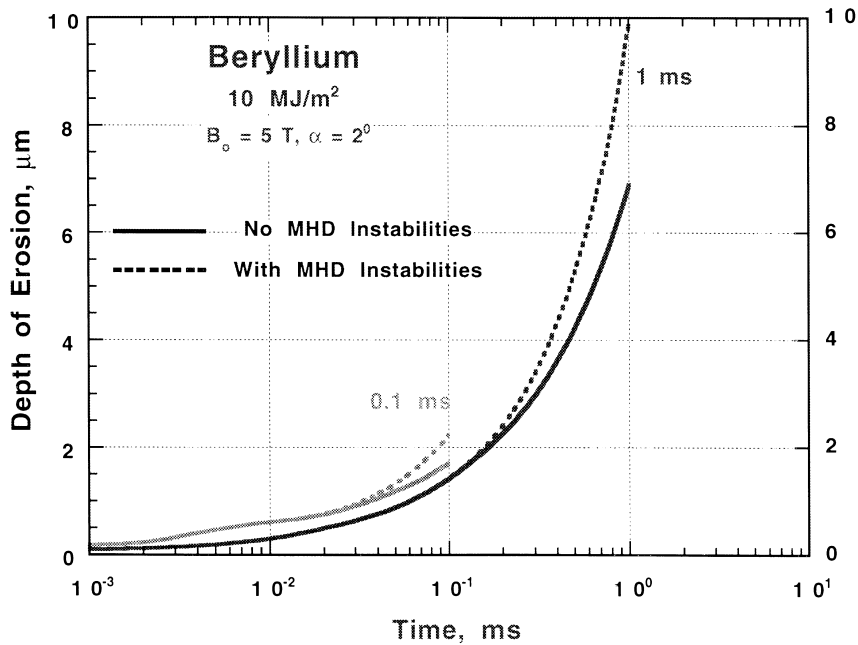
Fig. 4. Effect of MHD instabilities of beryllium erosion at two disruption times.

and nearby component geometry is needed. Such work is currently underway.

3. Erosion of metallic plasma-facing materials

Theoretical calculations have already shown that surface vaporization losses of metallic PFMS are small (only a few micrometers deep) over a wide range of plasma conditions during short plasma instabilities [3]. This is, again, due to the self-shielding mechanism, in which the material's own debris stops and absorbs most of the incoming plasma energy before it reaches the target surface. The net energy flux to the original disruption area is significantly reduced to <5% of its initial value, depending slightly on target material and the initial energy flux of the plasma [1]. This reduced energy flux is, however, high enough to cause significant melting of metallic PFCs and possible explosive-type erosion of CBMs over an extended exposure time. The resulting melt-layer thickness of metallic components can be one to two orders of magnitude higher than surface vaporization losses [2].

The surface of the developed melt layer is free to react to various existing forces during the disruption. Improved numerical models to study the dynamic erosion of the evolving melt layer that is due to various mechanisms and forces have been implemented in detail in the SPLASH code. These improved models in the SPLASH code have been coupled with the A*THER-MAL-S code, which calculates details of plasma/vapor interaction to more accurately predict melt-layer evolution, time-dependent melt erosion, and interaction with the developing vapor cloud.

Among the various mechanisms that can cause melt-layer erosion during plasma instabilities, two have been demonstrated experimentally and studied theoretically in detail [3,6]. One main mechanism observed in disruption simulation experiments is melt splashing due to the formation, growth, and bursting of bubbles inside the liquid layer. The second mechanism attributes erosion to the development and growth of hydrodynamic instabilities within the melt layer. The models of melt-layer erosion mechanisms are generally in good agreement with experimental data but slightly underestimate the average eroded depth at the higher energy densities of some simulation facilities [2]. This may suggest additional erosion mechanisms, such as those caused by a high incident plasma dynamic pressure in simulation experiments and the Raleigh–Taylor hydrodynamic instability due to inertial forces from the acceleration of the melt front at the solid/liquid interface [5].

Splashing due to volume bubble explosion is a result of the continuous heating and overheating of the liquid layer during energy deposition. Surface temperature of the liquid layer will exceed the equilibrium vaporization temperature for periods of time during plasma/material interaction. This overheating will lead to the growth and explosion or vaporization of volume bubbles as they reach the free surface. This explosion of bubbles, in turn,

leads to ejection and loss of parts of melt layer. The amount and rate of melt-layer erosion depend on many parameters, such as degree of overheating, impurity and gas content, material properties, and disrupting plasma parameters [14].

Hydrodynamic instabilities in the melt layer can develop during the thermal and current quench phases of a disruption as a result of plasma impact momentum (plasma wind) at the liquid surface and from forces generated by current decay in the liquid metal layer. During the thermal quench, part of the incident plasma momentum is absorbed in a thin surface layer of the liquid. This absorption will accelerate the liquid metal in this layer to very high velocities. As a result, a Kelvin–Helmholtz hydrodynamic instability will arise at the surface and form liquid droplets that will be transported away by the plasma wind [14].

In modeling melt-layer erosion in the SPLASH code, three different time-dependent behaviors were observed. Initially, most of the incoming plasma energy is directly deposited at the target surface, causing large overheating and the start of a splashing wave [14]. Soon after this, a shielding layer is developed and the power flux to the surface is significantly reduced and causes the liquid temperature to drop below the value that is necessary for splashing from bubble explosion due to heat conduction. Splashing from hydrodynamic instabilities is also reduced because the incident plasma momentum is partially absorbed by the shielding layer. This period of reduced splashing can be long and lasts up to several hundred microseconds [14]. After that, the liquid layer temperature starts to slowly rise again because of decreased heat conduction near the surface area. Splashing will then start again and the splashing velocity will be somewhat constant up to the end of the disruption.

Melt-layer erosion therefore depends on two main parameters: net power flux to the surface and disruption time. The net power flux to the surface in a typical disruption is $\approx$300–600 kW/cm^2, with slight dependence on initial power flux and target material. For a beryllium PFC and typical ITER disruption conditions of a net power flux to the surface of $S_{min} = 300$ kW/cm^2 and a disruption time of $\tau_d = 1$ ms, the calculated erosion depth is $\approx$200 μm. A sacrificial beryllium coating thickness of $\approx$5 mm thick, therefore, will only endure $\approx$25 disruptions; which is significantly less than the expected total number of disruptions of approximately several hundred during a reactor's lifetime.

During longer plasma instabilities, however, such as VDEs ($\tau_d \geqslant 100$ ms) or during deeper energy deposition, as in the case of runaway electrons, no significant self-shielding is expected to occur; therefore, serious erosion, melting, and structural damage can occur [1]. Longer plasma instabilities will also allow enough time for the deposited plasma energy to be conducted from the surface to the structural material and, finally, to the coolant channels where it can cause burnout [2]. Therefore, events such as VDEs and runaway electrons could have devastating effects than thermal quench disruptions, and their frequency should be drastically limited.

4. Erosion of carbon-based plasma-facing materials

Strong erosion with considerable mass losses that exceed those from surface vaporization is also observed for nonmelting materials, such as graphite and CBMs. The ejection of macroscopic particles (pieces) with illuminating tracks from CBM samples has been observed during electron beam irradiation in the JUDITH facility [8] and in plasma devices [10]. Recently, such strong erosion of CBMs was also observed during plasma flow interaction with graphite targets in the MKT facility at TRINITI [15]. Similar high erosion was also observed in laser and other facilities [16–18]. In most of these simulation facilities, the measured mass loss of graphite materials by surface vaporization was much greater than predicted, and the emitted particles were more macroscopic than particles emitted by monoatomic surface vaporization. The threshold energy necessary for mass loss is known to decrease from 60–100 kJ/cm^3 (monoatomic vaporization) to 20–40 kJ/cm^3 (mass losses in the form of macroscopic clusters such as $C_2, C_3, \cdots, C_n$). The dependence of mass loss on the incident heat flux and material properties, however, was not well studied in these facilities.

Existence of an exposure-time-dependent power threshold S_{min} for CBM destruction can be explained because at power levels of $<S_{min}$ graphite is only heated to temperatures $T_s < 3000$ K, which are not high enough for brittle destruction and spallation to take place. The strong erosion observed above $T_s > 3000$ K is commonly explained by the fact that binding energy between graphite particles (grains, crystallites) is sharply decreased. However, the existence of the S_{min} threshold may be explained by other recent mechanisms [14]. Such models for brittle destruction of graphite and CBMs are briefly discussed below.

One of the models used to explain brittle destruction is based on the assumption that the binding energy of grains and crystallites of graphite materials decreases sharply because of the high thermomechanical stresses that develop during the process [20,21]. During heating of CBMs to high temperatures and because of the high compressibility of the material structure, large thermomechanical stresses arise. Because of such large thermomechanical stresses, the grains of graphite are shifted and moved relative to each other and are cracked and divided into smaller pieces. Recently, however, new data cast doubt on thermomechanical forces as the only main mechanism for CBM destruction during short pulse exposure. For example, in experiments performed

at the GOL-3 facility, the path length of the (0.5–1) MeV electrons used in the simulation exceeded 500 μm, and all of the 500-μm layer was ejected from the exposed spot [17]. Even if all this layer is transformed into weakly bonded material by high thermomechanical stresses, it was not fully understood why such a large amount of material is completely ejected. Thermomechanical forces will produce large cracks that lead to brittle destruction of CBMs; however, the role that such forces play in total erosion requires further detailed studies. Another mechanism that explains the physics of CBM brittle destruction was recently developed [14] and briefly described below.

Usually, most graphite materials consist of grains and subgrains (crystallites) and exhibit a very porous structure. The size of graphite grains is ≈1–10 μm, with an intergranular boundary-layer of ≈0.1 μm. In addition, the grains consist of crystallites with size ≈100 Å, and intercrystallite boundary layers of size ≈10 Å. Pores exist in these intergranular and intercrystallite boundary layers in the form of small 'bubbles' that contain absorbed gases on the pore walls. During heating, these absorbed gases leave the surface and fill the pores. Under intense heating to high temperatures of a few thousand degrees, the pressure of the absorbed gases becomes very high ($P \approx 3000$ atm at $T \approx 3000$ K). Because of such high pressure, the grains, as in the case of thermomechanical stresses, are shifted and the grains are split into separate crystallites. Therefore, the material is transformed into a weakly bonded macroscopic dust. Further heating will lead to volume vaporization of this dust. Soon after the dust is vaporized, the pressure of both the gas and the vapor will eject the material. Such a model may help explain why volumetric heating (e.g., form electron beams) produces a hole formation. Given current and available data, it is difficult to evaluate the contribution of each mechanism to the net erosion of CBMs; in any case, explosive erosion is due to the pressure of both gas and vapor atoms and molecules inside the target material.

The energy of brittle destruction is a critical parameter in determining the net erosion rate of CBMs [14]. This value can be evaluated from the following considerations. The pressure of the saturated vapor must at least exceed the external pressure which is ≈10–50 atm during reactor disruption conditions. For $P_{out} = 10$ atm, the corresponding temperature of saturated vapor T_s, is ≈4000 K. Therefore, the required total energy is ≈12 kJ/cm³. In addition, some energy is necessary for complete brittle destruction and removal of material. For example, for chondritetype materials, this energy is ≈2–4 kJ/g or 4–8 kJ/cm³. For graphite, measurements of brittle destruction energy are not available in the open literature. If one assumes that the structure of graphite is similar to that of crumbly chondrites, one can estimate the total energy to be ≈16–20 kJ/cm³.

From experiments performed in the JUDITH facility, the total energy for brittle destruction is estimated to be ≈10 kJ/g after achieving the threshold of $T \approx 4000$ K [8]. In the GOL-3 experiment, from the spatial measurement of energy deposition and temperature rise, the erosion depth was close to the depth where energy deposition exceeded the value of 10 kJ/g for the MPG graphite [17]. This energy deposition corresponds to heating to a temperature of ≈3800–4000 K. Results from similar experiments performed at laser facilities do not contradict this estimate [18]. Therefore, from these experiments, the energy for brittle destruction of a graphite similar to the MPG-9 graphite is estimated to be ≈10 kJ/g or 20 kJ/cm³. Thus, for a net power flux to the material surface during a disruption of 300 kW/cm², the deposited energy for time $\tau_d = 1$ ms is $q = 0.3$ kJ/cm², which produces a net erosion of about 150 μm.

When compared with predicted values from pure surface vaporization (≈10 μm per disruption) this value is extremely high for graphite materials that are candidate for reactor coatings/tiles [22]. A sacrificial coating thickness of ≈1 cm could last <70 disruptions. This is, again, far less than the current expectations of approximately several hundred disruptions during a reactor lifetime. Therefore, more relevant experimental data and more detailed modeling are needed to evaluate the erosion of CBMs. Such models are currently being implemented in the SPLASH code [14].

5. Conclusion

Detailed aspects of plasma disruption and simulation physics have been studied by using comprehensive self-consistent models that integrate, in fine detail, the thermal evolution of a structure, as well as the physics of plasma/vapor interactions, MHDs and photon radiation transport in a multilayer structure. Theoretical predictions of A*THERMAL-S and SPLASH codes are generally in good agreement with various experimental results. Vapor-produced plasma and its confinement are important in further reducing disruption damage to the divertor plate and adjacent components. Loss of vapor plasma due to MHD instabilities, developed within the vapor layer, may increase divertor erosion, depending on the disrupting plasma parameters and divertor design. Photon radiation emitted from the vapor cloud, as well as the turbulent diffusing vapor, can also significantly damage nearby components. Both melt-layer splashing of metallic components and brittle destruction of CBMs are serious erosion mechanisms during various plasma instabilities. More detailed modeling and simulation experiments that are more relevant to reactors are required before a final decision is made about the selection of PFMs. In general, frequency of plasma instabilities in future tokamak machines must be sharply reduced to

only a few disruptions during a reactor lifetime. Moreover, the effects of redeposited debris from eroded and splashed materials on plasma contamination and subsequent reactor operations must be studied in detail.

Acknowledgements

References

[1] A. Hassanein, Fusion Technol. 30 (3) Part 2A (1996) 713.

[2] A. Hassanein et al., Materials effects and design implications of disruptions and off-normal events in ITER, Presented at Fourth International Symposium on Fusion Technology, 4–11 April 1997, Tokyo, Japan, to be published in Fusion Eng. Des.

[3] A. Hassanein, I. Konkashbaev, Suppl. J. Nucl. Fusion 5 (1994) 193.

[4] A. Hassanein, Fusion Technol. 26 (1994) 532.

[5] A. Hassanein, Fusion Technol. 15 (1989) 513.

[6] A. Hassanein et al., J. Nucl. Mater. 241–243 (1997) 288.

[7] V. Engelko et al., J. Nucl. Mater. 220–222 (1995) 1071.

[8] J. Linke et al., Fusion Technol. in: B. Keen, M. Huguet, R. Hemsworth (Eds.), 1991, p. 428.

[9] V.T. Astrelin et al., Fusion Technol. in: K. Herschbach, W. Maurer, J.E. Vetter (Eds.), 1994, p. 371.

[10] D.J. Den Hartog, R.D. Kendrick, J. Nucl. Mater. 220–222 (1995) 631.

[11] J. Gilligan et al., J. Nucl. Mater. 196–198 (1992) 596.

[12] A. Hassanein, I. Konkashbaev, Plasma Devices and Operations (1997) 1–17.

[13] N.I. Arkhipov et al., Fusion Technol. in: C. Varandas, F. Serra (Eds.), 1996, p. 507.

[14] A. Hassanein, I. Konkashbaev, L. Nikandrov, Argonne National Laboratory Report, ANL/FPP/TM-293, 1997.

[15] M. Gueseva et al., J. Technical Phys., to be published.

[16] J. Van der Iaan, J. Nucl. Mater. 162–164 (1989) 964.

[17] A.V. Burdakov et al., J. Nucl. Mater. 233–237 (1996) 697.

[18] R.C.L. van der Stad, H.Th. Klippel, G.J. Kraaij, Fusion Technol. in: C. Ferro, M. Gasparotto, H. Knoepfel (Eds.), 1992, p. 401.

[19] A. Yehia et al., J. Nucl. Mater. 233–237 (1996) 1266.

[20] R. Vassen, A. Kaiser, D. Stover, J. Nucl. Mater. 233–237 (1996) 708.

[21] O.V. Diyankov et al., Fusion Technol. (1997).

[22] A. Hassanein, I. Konkashbaev, J. Nucl. Mater. 233–237 (1996) 713.